Asian Journal of Chemistry; Vol. 37, No. 5 (2025), 1211-1223

ASIAN JOURNAL OF CHEMISTRY

https://doi.org/10.14233/ajchem.2025.33290

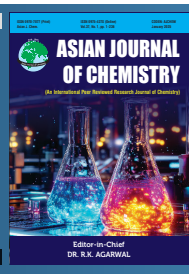

Mechanistic Molecular Insights and Quantum Biological Properties of Methyl-Imidazole Derivatives as Potential Anticancer Agents

SIMPLICE KOUDJINA[1,2,*], JOHN A. AGWUPUYE[3,*], TERKUMBUR E. GBER[3], MUHAMMAD ZEESHAN[4], PROVIDENCE B. ASHISHIE[3], SIDRA BATOOL[5], PRINCE DAVID[3], ELEONORE Y. LADEKAN[6] and GUY Y.S. ATOHOUN[2]

[1]National High School of Applied Biosciences and Biotechnologies (ENSBBA), National University of Sciences, Technology, Engineering and Mathematics (UNSTIM), BP 486 Abomey, Sogbo-Aliho, Benin
[2]Laboratory of Chemical Physics-Materials and Molecular Modeling, University of Abomey-Calavi (UAC), 03 BP 3409 Cotonou, Benin
[3]Department of Pure and Applied Chemistry, Faculty of Physical Sciences, University of Calabar, Calabar, Nigeria
[4]School of Pharmaceutical Sciences, Zhengzhou University, Zhengzhou, 450001, Henan, China
[5]Department of Chemistry, University of Okara, Okara-56300, Pakistan
[6]Laboratory of Physical Organic Chemistry and Synthesis, University of Abomey-Calavi (UAC), 02 BP 69 Bohicon, Benin

*Corresponding authors: E-mail: simplice.koudjina@unstim.bj; agwupuye.john@yahoo.com

Received: 30 December 2024; *Accepted*: 20 April 2025; *Published online*: 30 April 2025; AJC-21990

Methyl-imidazole derivatives are attracting considerable scientific attention because of their extensive and significant bioactivities. Hence, this work focuses on the investigation of the geometry, frontier molecular orbitals (FMOs), HOMO-LUMO energy gap, molecular docking, bioavailability, ADMET and pharmacokinetic properties of 1-(4-methoxyphenyl)-2,4,5-trimethyl-1*H*-imidazole (**M1**), 4-(4,5-dimethyl-1*H*-imidazol-1-yl)benzenesulfonic acid (**M2**), N-hydroxy-N-(4-(2,4,6-trimethyl-1*H*-imidazol-1-yl)phenyl)hydroxylamine (**M3**) and 2,4,5-trimethyl-1*H*-imidazole (**M4**) respectively, utilizing DFT at 6-311++g(d,p) basis set with different functionals *viz*. B3LYP, B3PW91, M062X, PBE0 and ωB967XD. A high-level quantum computational study and molecular docking were performed to ascertain the stability, reactivity and drug likeness of the titled molecules. Especially, compound **M2** had the least energy gap (3.92 eV) and its reactivity can be explained based on the attached sulphonic substituent compared to **M1**, **M3** and **M4**, respectively. Interestingly, the studied compounds showed good biological activities against various cancer proteins with PDB IDs 3F66, 4XVE, 1XF0 and 5Y8Y. The studied molecules present a valuable opportunity for developing cancer drugs with improved therapeutic indices.

Keywords: Methyl-imidazole derivatives, ADMET, Molecular docking, DFT.

INTRODUCTION

Several heterocyclic compounds containing nitrogen are rich in electron and they eagerly take or contribute a proton and can create varied weak interactions. These weak interactions can generate the intermolecular forces, such as hydrogenbonding formation, dipole-dipole interactions, hydrophobic effects, van der Waals forces and π stacking relations of nitrogen compounds, which make them important in the field of medicine [1]. It is worthy to note that the number and interaction of the chemical bonds influence the drug biological activity and toxicity. The flexibility in their bonding nature makes possible their binding with various enzymes and receptors in biological molecules with great affinity for electrons arising from their enhanced solubility. The operational features of their derivatives are advantageous since they display extensive bioactivities [2]. Heterocyclic compounds of methyl-imidazole derivatives have witnessed significant advancements in synthesis, theoretical studies, and applications, attributed to their diverse biological and pharmacological properties [3].

Imidazole consists of a five-member ring molecule that possesses a wide range of biological activities and is a vital pharmacophore in drug design [2]. Many Imidazole molecules have shown effectiveness as anticancer agents following their outstanding pharmaceutical potencies [4,5]. Amongst the notable features of imidazole is easy binding to DNA or protein components through diverse interactions, which include; intercalation, electrostatic and groove binding. The imidazole moiety

can be found in quite a lot of natural products like, alkaloids. Imidazoles are also a component of biological building blocks (*e.g.* histidine) and drugs [6]. In biological systems, imidazole and imidazolate are ligands to Zn^{2+} cation and their chelates are made up of the main active sites of a large class of metalloenzymes, which are part of fundamental bodily progressions [7], such as respiration, photosynthesis or acid-base balance of all living organisms [8]. Methyl-imidazole derivatives are also deployed as corrosion inhibitors [9].

Computational studies are employed to stream line the window of the applications of this prospective candidate through prediction of the most important reactive properties which helps in reducing experimental cost by proffering precise methods for experimental achievements [10,11]. In present work, we make insights into the biological activities/properties of methyl-imidazole derivatives using density functional theory (DFT). Molecular modeling studies have influenced the formation and understanding of the role of ligands and metal-ligand complexes in biological systems. Density functional theory (DFT) along with *ab initio* methods like Moller Plesset second order perturbation (MP2) has shown complementary synergy in the study of biological activities of imidazole and its derivatives. Still, B3LYP, MP2, PW9I, BLYP have predicted the intermolecular interaction energy for a series of imidazole dimers [12]. These benchmarking tools showed mean signed errors (MSE) [13-18].

B3LYP is the most widely used density-functional theory (DFT) approach because it is capable of accurately predicting molecular structures and other properties. Yet the B3LYP has its limitation/drawbacks as in most cases it is not able to reliably model systems in with non-covalent interactions [19]. One of the leading importance of the exertions of comparative studies in functionals influence on covalent and non-covalent relations is that it plays a key role in the science world oscillating from biochemistry to condensed matter physics and various schemes of interest by lowering cost estimate for computational modelling [20].

A study by Asogwa *et al.* [21] comparing the following functions PBEPBE, ωB97XD and B3PW91, has shown that arising from NBO, the charge transfer arising from the delocalization of electrons on systems and hyperconjugative interaction amid bonds is most significant with PBEPBE due to its great energy of stabilization, which accounts for the compound stability, indicating strong interaction between atoms in bond distances [18]. In this study, a spectrum of exchange correlation functionals is explored to ascertain precision and accuracy in computational studies of the modeled nitrogen heterocycles (imidazole). This is necessary here because, majority of practical DFT applications are based on hybrid functionals, which provide the best compromise between accuracy and computational efforts [22]. Furthermore, the modelled compounds screen by employing molecular docking to ascertain their biological activities against various cancer proteins.

COMPUTATIONAL METHODS

All computational quantum calculations were carried out by employing diverse software, which includes Gaussian16W [23] with GaussView.6.0.16 [24], FMOs using the Koopmans approximation [25], molecular docking, natural bond orbital analysis as well as the ADMET properties. The analysis of the electronic properties of the modelled molecules was carried out using density functional theory. In any case, it is always appropriate to ascertain the performance of the DFT methods used in studies of this kind hence, B3PW91 [26], B3LYP [27], M06-2X [28] and PBEPBE [29] in 6-311++g(d,p) basis set was utilized in the geometries optimized structures. The frontier molecular orbitals (FMOs) showing the energy gap was calculated using the same method of theory and basis set and the energy level was estimated by carrying out the natural bond orbital (NBO) calculations [30,31]. *In silico* molecular studies were carried out to assess the binding interactions between the title molecules (Fig. 1) and the targeted cancer proteins. Indeed, the biological activities of methyl-imidazole derivatives (**M1-M4**) against various cancer proteins having PDB IDs as 3F66, 4XVE, 1XF0 and 5Y8Y, which would be used for molecular docking investigation. These biological activities of cancer proteins were enhanced by interactions with the methyl-imidazole derivatives (**M1-M4**) and the structures of the optimized compounds were obtained and saved in PDB format. Molecular docking calculations were done using SeeSAR.12.1.0 software program [32] to screen the biological activities of the title molecules against various cancer proteins.

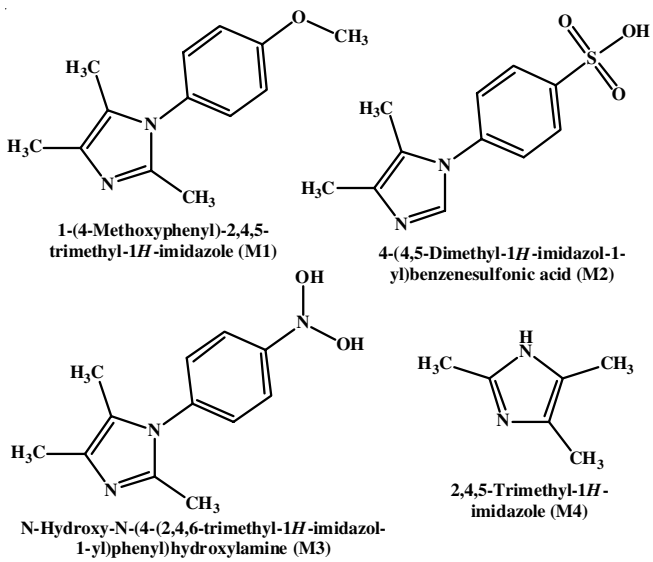

Fig. 1. Structures of methyl-imidazole derivatives (**M1-M4**)

Prediction of pharmacokinetic properties: The ADMET online tool (https://admetmesh.scbd.com/service/evaluation/cal) was employed to evaluate the absorption, distribution, metabolism, excretion and toxicity (ADMET) characteristics of the methyl-imidazole derivatives (**M1-M4**). The results served as valuable indicators for predicting the pharmacokinetic properties of compounds [33].

Drug-likeness and ADMET analysis: Drug-likeness is a crucial component of pharmacological development since it allows for the quick screening of drug compounds. Based on the ADMET (https://admetmesh.scbdd.com/) program, the

methyl-imidazole derivatives were evaluated for their drug-like nature using Lipinski's rules of five. According to the Lipinski's criterion, "drug-like" molecules should have a LogP of less than 5, a molecular weight (M.W.) below 500, a total polar surface area under 140 and an equal number of hydrogen bond acceptors (HBA) and donors (HBD) below 10 and 5 [34].

The ADMET laboratory web platform was utilized to assess a range of pharmacokinetic properties of methyl-imidazole derivatives (**M1**-**M4**) within the human organism, encompassing absorption, distribution, metabolism, excretion and toxicity. The ADMET lab took into account numerous factors, including human intestinal absorption (HIA+ or HIA-), blood-brain barrier penetration (BBB+ or BBB-), Caco-2 permeability (permeable or non-permeable), human hepatotoxicity (H-HT), Solubility (as denoted by the LogS value) and acute toxicology.

Evaluation of ADMET parameters and drug-likeness: For the drug-likeness assessments based on specific rules like Lipinski's rule, Pfizer's rule, GSK's rule and the Golden triangle rule, the physico-chemical properties of the compounds were typically examined and related to some filter versions.

RESULTS AND DISCUSSION

Molecular geometries: To enhance a deeper understanding on the inter- and intra-atomic interaction, the stability and reactivity of the studied compound in relation to its biological applications. Molecular geometry is very curial analysis to be performed. Hence energy minimization otherwise referred to as structural optimization was performed at DFT using five different functional to elucidate the claim that climbing the Jakobi Ladder of functionals increases the accuracy [35,36]. The DFT/B3LYP, B3PW91, M062X, PBE0, ωB967XD functional with 6-311++G(d,p) basis set were used to achieved the optimized ground state molecular structure. Geometry parameter analysis including bond length and bond angle of the studied compounds (**M1**, **M2**, **M3** and **M4**) were theoretically investigated. 2,2,5-Trimethyl-2,5-dihydro-1*H*-imidazole (**M4**) was substituted with different functional groups to understand the influence of the attached functional groups on the reactivity and geometry morphological properties of the studied compounds. According to the extensive literature surveys, the experimental X-ray results of the studied compounds have been reported [37] and it is important to mentioned that the experimental values are typically obtained in solid state, whereas theoretical values are derived in gas phase. Theoretical influence based on the different employed functional couple with the fact the weak interaction normally occurs in solid state material, the calculated bond length and angle presented herein are slightly higher compared to previously reported values in literature [38]. Importantly, the concept bond length is described as the distance between the nuclei of two bound atoms and it is impacted by a number of elements such as the atom types involved in the bond, the bond order and the surrounding environment [39,40]. On the other hand, the bond angle is the angle formed by two neighbouring bonds in a molecule [41]. According to Fig. 2, it can be shown that the title compounds' aromatic ring modifications are remarkably affected by substituents' effects on other molecular properties. For instance, it was found that the influence of the various substituent attachments gradually changed the bond length and bond angle of the title molecular (**M1**, **M2**, **M3** and **M4**) of methyl substituted on the imidazole

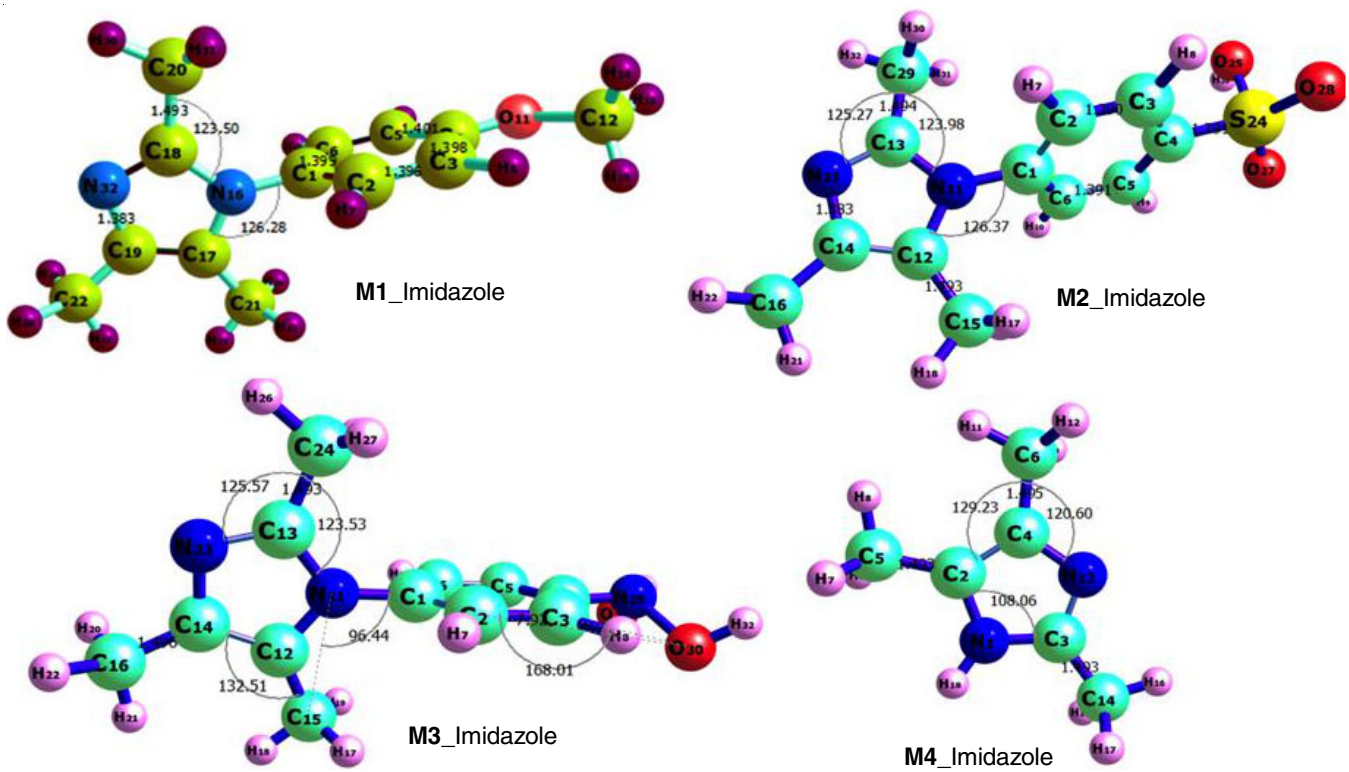

Fig. 2. Optimized geometry parameters including the bond length and bond angle of methyl-imidazole derivatives (**M1**, **M2**, **M3**, **M4**) theoretically predicted

bond length form C18–C20 (1.493) in case of **M2** C13-29 (1.496), **M3** C13–C24 (1.493) and **M4** C4–C6 (1.495) and all other bonds of the examined compounds. A comparable observation was observed regarding the bond angle, indicating that modifications to the aromatic ring of compounds are significantly influenced by the effects of substituents on various molecular properties. Hence, this analysis can be used in forecasting the characteristic of molecules and can give valuable knowledge about their reactivity and characteristics.

Frontiers molecular orbitals (FMOs) and global reactivity descriptors: At this level of quantum description, Fig. 3 present information about the frontier molecular orbitals of the

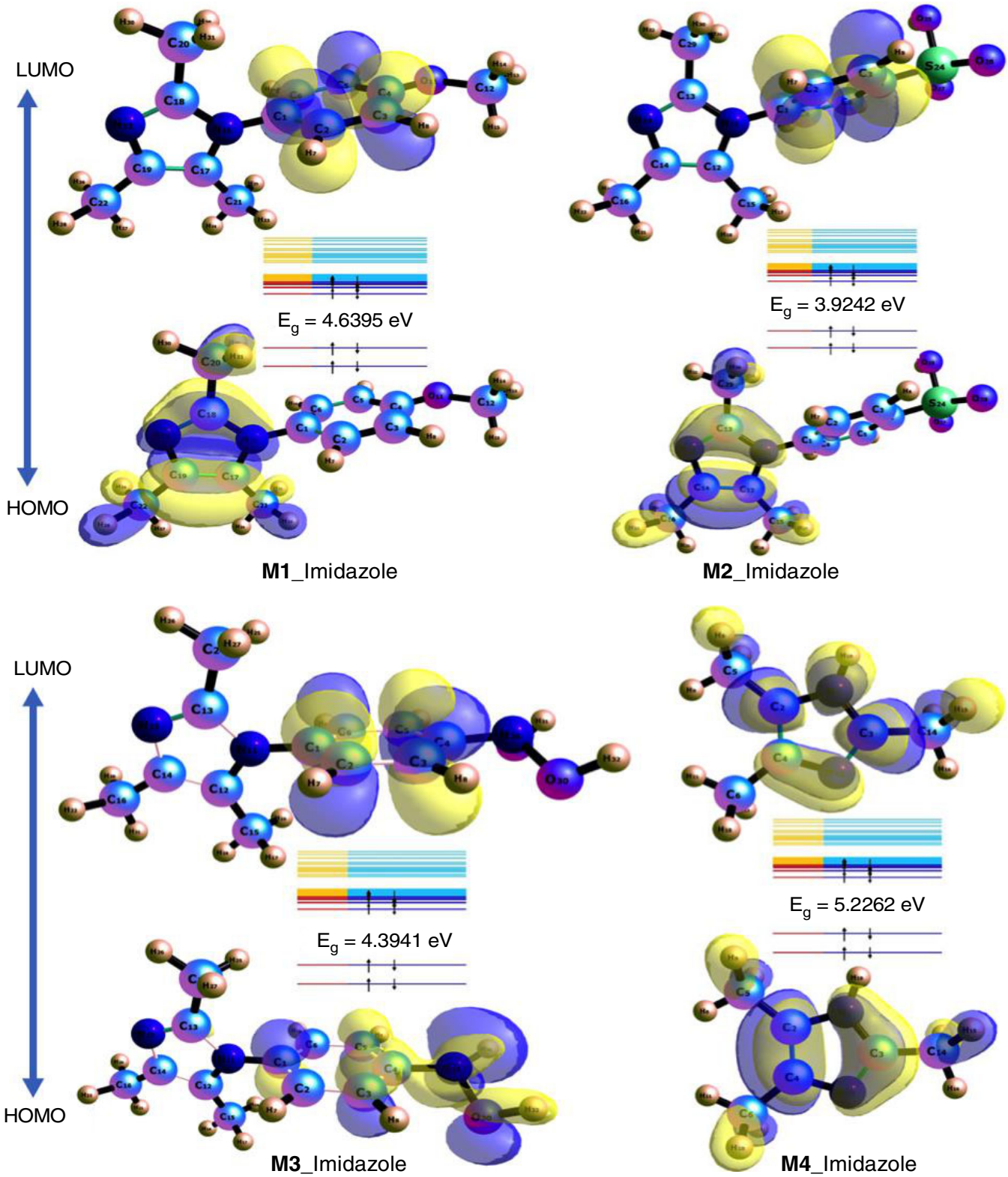

Fig. 3. HOMO, LUMO isosurface of methyl-imidazole derivatives (**M1**, **M2**, **M3**, **M4**) obtained at B3LYP/6-311G++(d,p) level of theory

studied molecules (**M1**, **M2**, **M3**, **M4**) at five different theoretical methods DFT/B3LYP, B3PW91, M062X, PBE0, ωB967XD functional with 6-311++G(d,p) basis set. In chemistry, the highest occupied molecular orbital (HOMO) and lowest unoccupied molecular orbital (LUMO) of a molecule are referred to as border molecular orbitals [42,43]. These orbitals are crucial in determining a molecule's reactivity and other characteristics in relation to its applications [44]. Electron transfer begins with the HOMO, which represents the electron density susceptible to chemical processes. LUMO is the electron density most likely to accept electrons in a chemical process. LUMO is the orbital to which electrons are accepted, making it the "end point" for electron transfer in chemical processes [45,46]. The HOMO-LUMO energy gap or HOMO-LUMO gap refers to the energy differential between the HOMO and LUMO:

$$E_{gap} = E_{LUMO} - E_{HOMO} \quad (1)$$

This energy gap is very crucial in analyzing and interpreting the ease with which a molecule can give or take electrons in a chemical process. Hence literature review has it that the molecule is more reactive when the HOMO-LUMO gap is smaller on the other hand the stability of a studied species is associated by the larger the energy gap [47,48]. From the result presented in Table-1, it can be observed that the reactivity and stability of the studied compounds are affected by the aromatic ring modifications due to the effects of substituents on other molecular properties. In like manner, the reactivity and stability of the studied compound (**M1**-**M4**) was observed at different theoretical methods thus; For **M1**; **M1**_ωB9XD > **M1**_M06-2X > **M1**_PBE1PBE > **M1**_B3PW91 > **M1**_B3LYP with the respective energy gap values of 6.6573 > 6.5686 > 5.0115 > 4.6542 > 4.6395 eV, respectively. This is an indication that the studied molecule is more stable at the ωB9XD method of theory. Similar observed was made in all the studied structures as presented in Table-2. Hence, it can be inferred that the higher the functional, the more stable the structure and the less reactive the compound in the biological systems. However, comparing the studied compounds in terms of energy gap, it was observed that compound **M2** had the least energy gap (3.92 eV) and its reactivity can be explained based on the attached sulphonic substituent. Also, the highest energy gap obtained was from the parent compound **M4** with an energy value of 5.23 eV and can be explain on the basis of the ability of the electron dense region in the title molecule. Lack of the aromatic ring attachment could also be the reason for the stability of the titled compounds. Order of reactivity to the biological system of the studied compound can be arranged in decreasing order thus: **M2**_B3LYP > **M3**_B3LYP > **M1**_B3LYP > **M4**_B3LYP that is (**M2** > **M3** > **M1** > **M4**). From Fig. 3, the HOMO–LUMO isosurface of the studied compounds is depicted, it was observed that in **M1**, the HOMO was highly concentrated at the imidazole ring whereas the LUMO was delocalized on the substituted benzene ring. Similar observation was made for compound **M2**. Moreover, for **M3**, the LUMO was delocalized at the benzene ring but the HOMO was concentrated on the attached substituent. All the global reactivity descriptors were described as follow:

$$IP \approx -E_{HOMO} \text{ and } EA \approx -E_{LUMO} \quad (2)$$

Electronegativity index:

$$\chi = -\frac{[E_{HOMO} + E_{LUMO}]}{2} \quad (3)$$

Hardness:

$$\eta = \frac{[E_{LUMO} - E_{HOMO}]}{2} \quad (4)$$

Softness:

$$\sigma = \frac{1}{2\eta} \quad (5)$$

TABLE-1
SOME ELECTRONICS PARAMETERS OF METHYL-IMIDAZOLE DERIVATIVES (**M1**, **M2**, **M3**, **M4**) IN (eV), CONSIDERING SEVERAL DENSITY FUNCTIONALS

Compounds	HOMO	LUMO	E_{gap}	IP	EA	μ	η	ω
M1_B3LYP	-5.56	-0.92	4.64	5.56	0.92	-3.24	2.32	12.16
M1_B3PW91	-5.56	-0.91	4.65	5.56	0.91	-3.23	2.33	12.15
M1_M06-2X	-6.88	-0.31	6.57	6.88	0.31	-3.59	3.28	21.19
M1_PBE1PBE	-5.72	-0.71	5.01	5.72	0.71	-3.21	2.51	12.95
M1_ωB9XD	-7.52	-0.86	6.66	7.52	0.86	-3.33	4.19	23.22
M2_B3LYP	-6.05	-2.12	3.92	6.05	2.12	-4.08	1.96	16.36
M2_B3PW91	-6.05	-2.12	3.93	6.05	2.12	-4.08	1.97	16.39
M2_M06-2X	-7.37	-1.16	6.21	7.37	1.16	-4.27	3.11	28.29
M2_PBE1PBE	-6.22	-1.90	4.31	6.22	1.90	-4.06	2.16	17.79
M2_ωB9XD	-7.99	-0.22	7.78	7.99	0.22	-4.10	3.89	32.75
M3_B3LYP	-5.58	-1.19	4.39	5.58	1.19	-3.39	2.19	12.59
M3_B3PW91	-5.58	-1.06	4.52	5.58	1.06	-3.32	2.26	12.42
M3_M06-2X	-6.90	-0.58	6.32	6.90	0.58	-3.74	3.16	22.12
M3_PBE1PBE	-5.74	-0.90	4.84	5.74	0.90	-3.32	2.42	13.34
M3_ωB9XD	-7.54	-0.63	6.92	7.54	0.63	-4.08	3.46	28.83
M4_B3LYP	-5.71	-0.49	5.23	5.71	0.49	-3.10	2.61	12.56
M4_B3PW91	-5.71	-0.22	5.49	5.71	0.22	-2.97	2.75	12.08
M4_M06-2X	-7.01	-0.29	6.72	7.01	0.29	-3.65	3.36	22.41
M4_PBE1PBE	-5.87	-0.24	5.63	5.87	0.24	-3.05	2.81	13.12
M4_ωB9XD	-7.67	-0.92	6.76	7.67	0.92	-4.29	3.38	31.13

TABLE-2
SECOND ORDER PERTURBATION THEORY ANALYSIS OF FOCK MATRIX IN NBO BASIS OF METHYL-IMIDAZOLE DERIVATIVES (**M1**, **M2**, **M3**, **M4**), CONSIDERING SEVERAL DENSITY FUNCTIONALS

	Donor	Acceptor	E^2 (kcal/mol)	E(j)-E(i) (a.u)	F(i,j)
M1-B3LYP	πC3-C4	π*C5-C6	290.81	0.01	0.08
M1-B3PW91	πC3-C4	π*C5-C6	291.67	0.01	0.08
M1-M06-2X	πC3-C4	π*C5-C6	311.69	0.01	0.09
M1-PBE1PBE	πC3-C4	π*C5-C6	305.66	0.01	0.09
M1-ωB97XD	πC3-C4	π*C1-C2	453.87	0.01	0.10
M2-B3LYP	πC4-C5	π*C1-C6	292.53	0.01	0.09
M2-B3PW91	πC4-C5	π*C1-C6	302.65	0.01	0.09
M2-M06-2X	πC4-C5	π*C1-C6	379.44	0.01	0.13
M2-PBE1PBE	πC4-C5	π*C1-C6	322.38	0.01	0.09
M2-ωB97XD	πC4-C5	π*C1-C6	334.74	0.02	0.11
M3-B3LYP	πC13-N23	π*C12-C14	57.07	0.03	0.06
M3-B3PW91	πC13-N23	π*C12-C14	60.41	0.03	0.06
M3-M06-2X	πC13-N23	π*C12-C14	88.82	0.02	0.07
M3-PBE1PBE	πC13-N23	π*C12-C14	64.30	0.03	0.06
M3-ωB97XD	πC13-N23	π*C12-C14	77.81	0.03	0.08
M4-B3LYP	πC3-N13	π*C2-C4	57.85	0.03	0.06
M4-B3PW91	πC3-N13	π*C2-C4	61.60	0.03	0.06
M4-M06-2X	πC3-N13	π*C2-C4	89.93	0.02	0.07
M4-PBE1PBE	πC3-N13	π*C2-C4	65.51	0.03	0.06
M4-ωB97XD	πC3-N13	π*C2-C4	79.40	0.03	0.08

Chemical potential:

$$\mu = \frac{[E_{LUMO} + E_{HOMO}]}{2} \quad (6)$$

Electrophilicity index:

$$\omega = \frac{\mu^2}{2\eta} \quad (7)$$

These different descriptors were calculated from the studied compounds using the population Koopmans' approximation to further analyze the chemical stability and reactivity [49]. The frontier molecular orbital gap of the analyzed derived compounds was found to be in excellent accord with the calculated quantum descriptors. From the global descriptors presented herein another crucial quantum reactivity notion utilized to comprehend the electrophilicity of molecular systems is the global electrophilicity index (ω). The higher the electrophilicity index value, the more electrophilic the system. In other words, the electrophilicity index is a critical measure that helps in establishing the toxicity of compounds by assessing the biological activity of the drug-receptor interaction.

Natural orbital bond (NBO) analysis: The study of charge transfer from the lone pair and π-electrons of an atom to the anti-bonding orbitals of another atom is referred to as NBO analysis [50]. Its capacity to interpret chemical interactions and complex reactivity in molecular systems has been proven, alongside being a convenient instrument for the examination of delocalization of electron density, hyperconjugation effects and measuring intermolecular and intra-molecular interactions [51]. Second-order perturbation theory was employed for determining the energetic significance of NBOs, which considers all plausible interactions between filled donor and empty acceptor NBOs. The second order stabilization energy of three functional with electron delocalization between donor and acceptor of each donor NBO(i) and acceptor NBO(j) is predicted to be each donor NBO(i) and acceptor NBO(j) using:

$$E^{(2)} = q_i \frac{(F_{ij})^2}{E(i) - E(j)}$$

where q_i represents orbital occupancy; F_{ij} is the off-diagonal element on folk matrix; E(j) − E(i) is the diagonal elements and $E^{(2)}$ represents the second order stabilization energy of the system and E(j) − E(i) represents the orbital energy differences of the donor and acceptor of NBO. Table-2 shows the NBO analysis of B3LYP, B3PW91, M06-2X, PBE1PBE and ωB97XD and donor and acceptor interaction for four compounds **M1**, **M2**, **M3** and **M4**. The more powerful the connection between electron donors and the greater the level of conjugation of the whole system is the higher the stabilization energy value (E^2). For **M1**, with the stabilization energy of natural bond orbitals of 453.87 kcal/mol for ωB97XD, the investigated compound demonstrated the most important donor-acceptor NBO interactions between π*C3–C4 and π*C1–C2 indicating strong interaction between the Lewis donor and Lewis acceptor charge transfer. B3LYP, B3PW91, M06-2X and PBE1PBE also show donor and acceptor interactions of π*C3–C4, π*C5–C6, π*C3–C4, π*C5–C6 and π*C3–C4, π*C5–C6 and π*C3–C4, π*C5–C6 with the stabilization energy of 290.81 kcal/mol, 291.67 kcal/mol, 311.69 kcal/mol and 305.66 kcal/mol, respectively, indicating that B3LYP had very little interaction with the donor orbitals. For **M2**, with the stabilization energy of natural bond orbitals of 379.44 kcal/mol for M06-2X, the investigated compound demonstrated the most important donor-acceptor NBO interactions between π*C4–C5 and π*C1–C6 indicating strong interaction between the Lewis donor and Lewis acceptor charge transfer. B3LYP, B3PW91, PBE1PBE and ωB97XD all show

donor and acceptor interactions of π*C4–C5, π*C1–C6 with the stabilization energy of 292.53 kcal/mol, 302.65 kcal/mol, 322.38 kcal/mol and 334.74 kcal/mol respectively, indicating that B3LYP again had very little interaction with the donor orbitals. For **M3**, with the stabilization energy of natural bond orbitals of 88.82 kcal/mol for M06-2X, the investigated compound demonstrated the most important donor-acceptor NBO interactions between π*C13–N13 and π*C12–C14 indicating strong interaction between the Lewis donor and Lewis acceptor charge transfer. B3LYP, B3PW91, PBE1PBE and ωB97XD all show donor and acceptor interactions of π*C13–N13, π*C12–C14 with the stabilization energy of 57.07 kcal/mol, 60.41 kcal/mol, 64.30 kcal/mol and 77.81 kcal/mol respectively, indicating that B3LYP had very little interaction with the donor orbitals. For **M4**, with the stabilization energy of natural bond orbitals of 89.93 kcal/mol for M06-2X, the investigated compound demonstrated the most important donor-acceptor NBO interactions between π*C1–N13 and π*C2–C4 indicating strong interaction between the Lewis donor and Lewis acceptor charge transfer. B3LYP, B3PW91, PBE1PBE and ωB97XD all show donor and acceptor interactions of π*C1–N13, π*C2–C4 with the stabilization energy of 57.85 kcal/mol, 61.60 kcal/mol, 65.51 kcal/mol and 79.40 kcal/mol respectively, indicating that B3LYP had very little interaction with the donor orbitals.

Molecular docking studies: By leveraging this approach, researchers can efficiently navigate the intricate landscape of molecular interactions, facilitating the identification of promising targets for further exploration and potential therapeutic interventions [52-54]. To assess the binding interactions between the titled molecules and the targeted cancer proteins, *in silico* molecular studies become necessary and which is also crucial in drug discovery and development process [55]. The biological activity values of the methyl-imidazole derivatives (**M1-M4**) against various cancer proteins having PDB IDs 3F66 [56], 4XVE [57], 1XF0 [58] and 5Y8Y [59] were calculated in this work utilizing the molecular docking approach. These cancer proteins' biological activities were enhanced by interactions with the methyl-imidazole derivatives (**M1-M4**). The structures of the optimized compounds were obtained using the Gaussian software and saved in PDB format. Molecular docking calculations was done using SeeSAR.12.1.0 software program to screen the biological activities of the molecules against various cancer proteins.

Hepatocyte growth factor receptor (3F66), bromodomain containing protein (5Y8Y), aldo-keto reductase family 1 member C3 (1XF0) and β-hydroxysteroid dehydrogenase (4XVE) had their molecular docking HYDE energy values computed. The biological activity values of 1-(4-methoxy-phenyl)-2,4,5-trimethyl-1*H*-imidazole (**M1**) for cancer proteins with PDB IDs 1XF0, 3F66, 4XVE and 5Y8Y were determined to be -19.7, -5.0, -6.4 and 23.2 KJ mol^{-1}, respectively, when the HYDE binding scores were investigated. The binding pose of **M1** in cancer proteins is shown in Fig. 4. According to the calculations, these values for 4-(4,5-dimethyl-1*H*-imidazol-1-yl)-benzene sulfonic acid (**M2**) are -16.5 for 1XF0, -17.1 for 3F66, -13.5 for 4XVE and 15.2 kJ mol^{-1} for 5Y8Y. The representation of the binding interaction is shown in Fig. 5. Indeed, *N*-hydroxy-N-(4-(2,4,6-trimethyl-1*H*-imidazol-1-yl)phenyl)hydroxylamine (**M3**) was found to dock inside the active pocket 1XF0, 3F66, 4XVE and 5Y8Y with binding affinities (HYDE scores) of -9.9, -7.9, -14.3 and -15.4 kJ mol^{-1}, respectively and its binding interaction in cancer proteins a shown in Fig. 6. Docking of 2,4,5-trimethyl-1*H*-imidazole (**M4**) inside the 1XF0, 3F66, 4XVE and 5Y8Y gave the binding affinities of -21.0, -16.0, -10.4 and -15.1 kJ mol^{-1} respectively. The binding pose of **M4** in cancer proteins is shown in Fig. 7.

When the HYDE energy parameter was calculated using molecular docking, the biological activity values of methyl-imidazole derivatives (**M1**-**M4**) were compared. According to the calculations, **M4** has the highest biological activity among them. However, **M3** has the lowest biological activity. HYDE energy values of the methyl-imidazole derivatives (**M1-M4**) against the four cancer proteins are summarized in Table-3.

TABLE-3
MOLECULAR DOCKING BINDING AFFINITIES (HYDE SCORES) IN kJ mol^{-1} FOR METHYL-IMIDAZOLE DERIVATIVES (**M1-M4**) AGAINST CANCER PROTEINS

Compounds	1XF0	3F66	4XVE	5Y8Y
M1	-19.7	-5.0	-6.4	-23.2
M2	-16.5	-17.1	-13.5	-15.2
M3	-9.9	-7.9	-14.3	-15.4
M4	-21.0	-16.0	-10.4	-15.1

For 1XF0, biological activity of methyl-imidazole derivatives was **M4 > M1 > M2 > M3**, for 3F66, it was **M2 > M4 > M3 > M1**, for 4XVE, it was **M3 > M2 > M4 > M1** and for 5Y8Y, it was **M1 > M3 > M2 > M4**. The main factor contributing to a compound's enhanced biological activity is its larger area of contact relative to other molecules of interest; as the surface area of contact increases, so does the biological activity value [60,61]. The interaction between molecules and proteins is enhanced by increased molecule contact surface.

ADMET parameters and drug-likeness: The primary obstacle, which typically pertains to ADMET properties and different toxicities, may be explained by limitations in efficacy and safety, as well as non-technical issues. As a result, the physicochemical radar chart of the methyl-imidazole derivatives (**M1-M4**) was produced from the ADMET lab 2.0 online servers. Brown Area: Each property's upper limit compound property is shown in blue and the Bioavailability property's lower limit is shown in pink (Fig. 8).

The majority of the compounds exhibit physico-chemical characteristics that align with the upper limit, as indicated by the brown colour. The methyl-imidazole derivatives (**M1**-**M4**) has been subjected to the Lipinski's rule of five and the results are presented in Tables 4 and 5. Lipinski's criteria for drug-likeness include parameters such as molecular weight (MW 500 g/mol), *n*-octanol/water distribution coefficient (LogP5), number of hydrogen bond acceptors (nHA 10) and number of hydrogen bond donors (nHD 5). Notably, the methyl-imidazole derivatives (**M1**-**M4**) demonstrate commendable performance when compared to the ideal threshold ($0 < \text{LogP} < 3$). This finding suggests that these modeled compounds possess favourable oral bioavailability and water solubility [62].

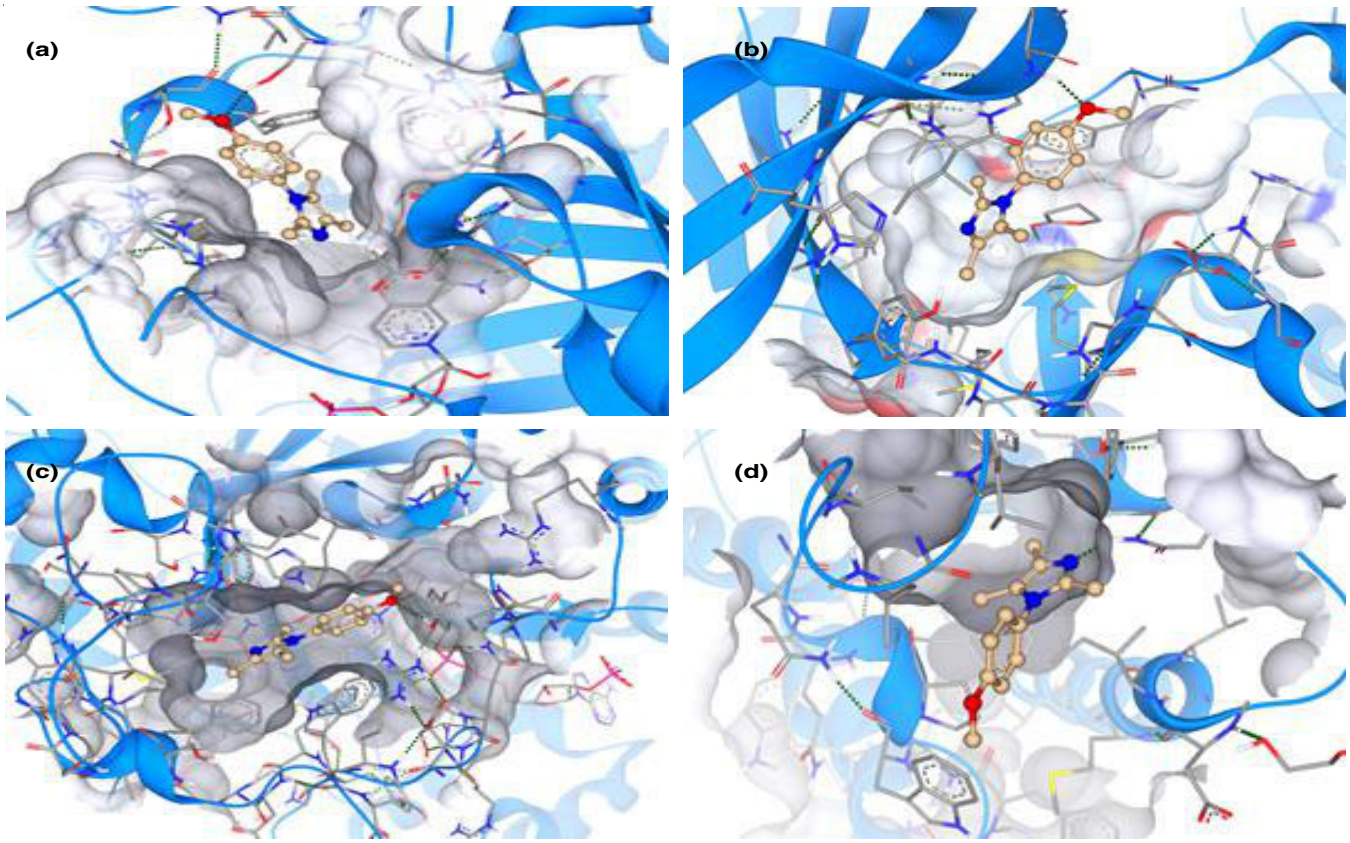

Fig. 4. Representation of the interaction from 1-(4-methoxyphenyl)-2,4,5-trimethyl-1*H*-imidazole (**M1**) with (a) 1XF0, (b) 3F66, (c) 4XVE and (d) 5Y8Y

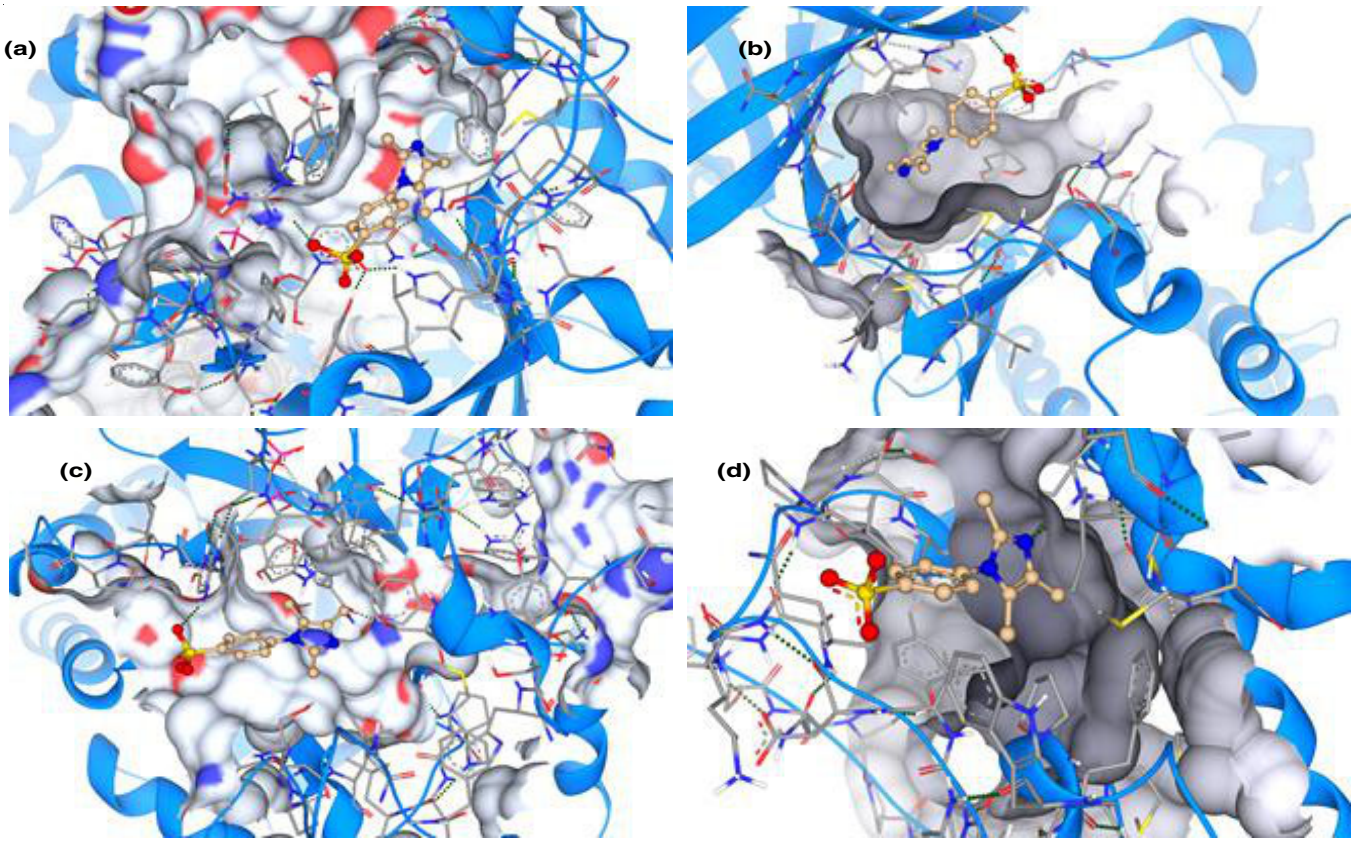

Fig. 5. Representation of the interaction from 4-(4,5-dimethyl-1*H*-imidazol-1-yl)benzenesulfonic acid (**M2**) with (a) 1XF0, (b) 3F66, (c) 4XVE and (d) 5Y8Y

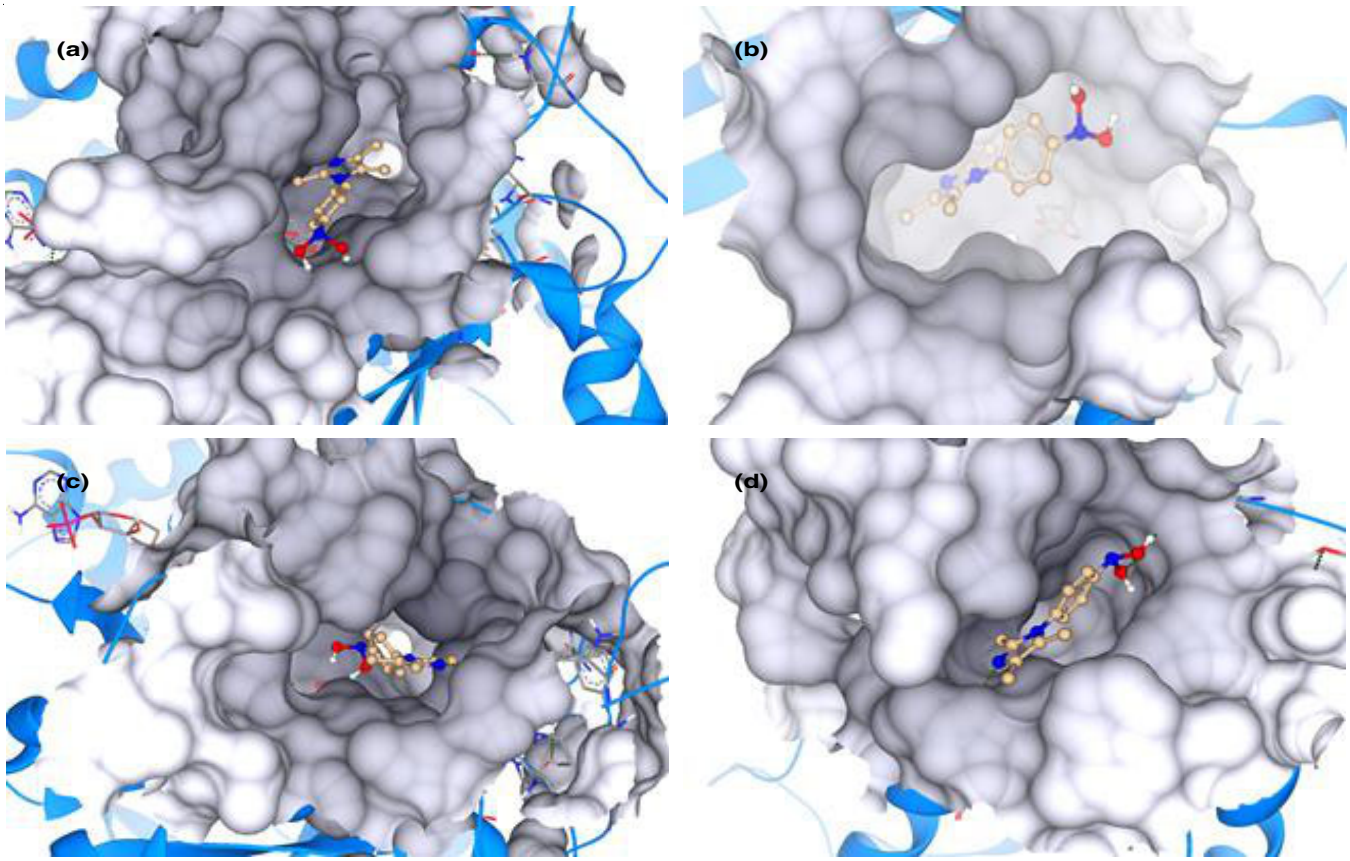

Fig. 6. Representation of the interaction from N-hydroxy-N-(4-(2,4,6-trimethyl-1*H*-imidazol-1-yl)phenyl)hydroxylamine (**M3**) with (a) 1XF0, (b) 3F66, (c) 4XVE and (d) 5Y8Y

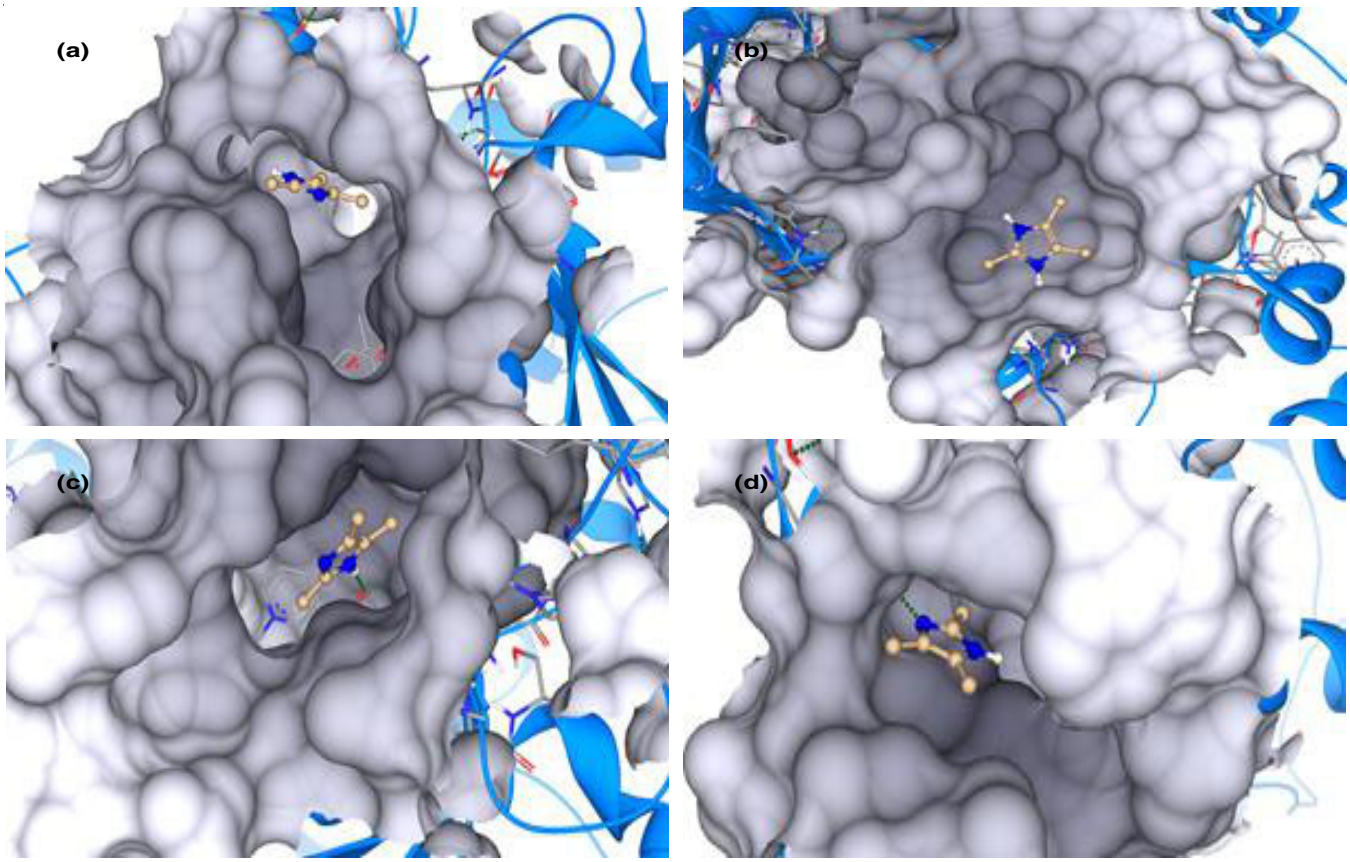

Fig. 7. Representation of the interaction from 2,4,5-trimethyl-1*H*-imidazole (**M4**) with (a) 1XF0, (b) 3F66, (c) 4XVE and (d) 5Y8Y

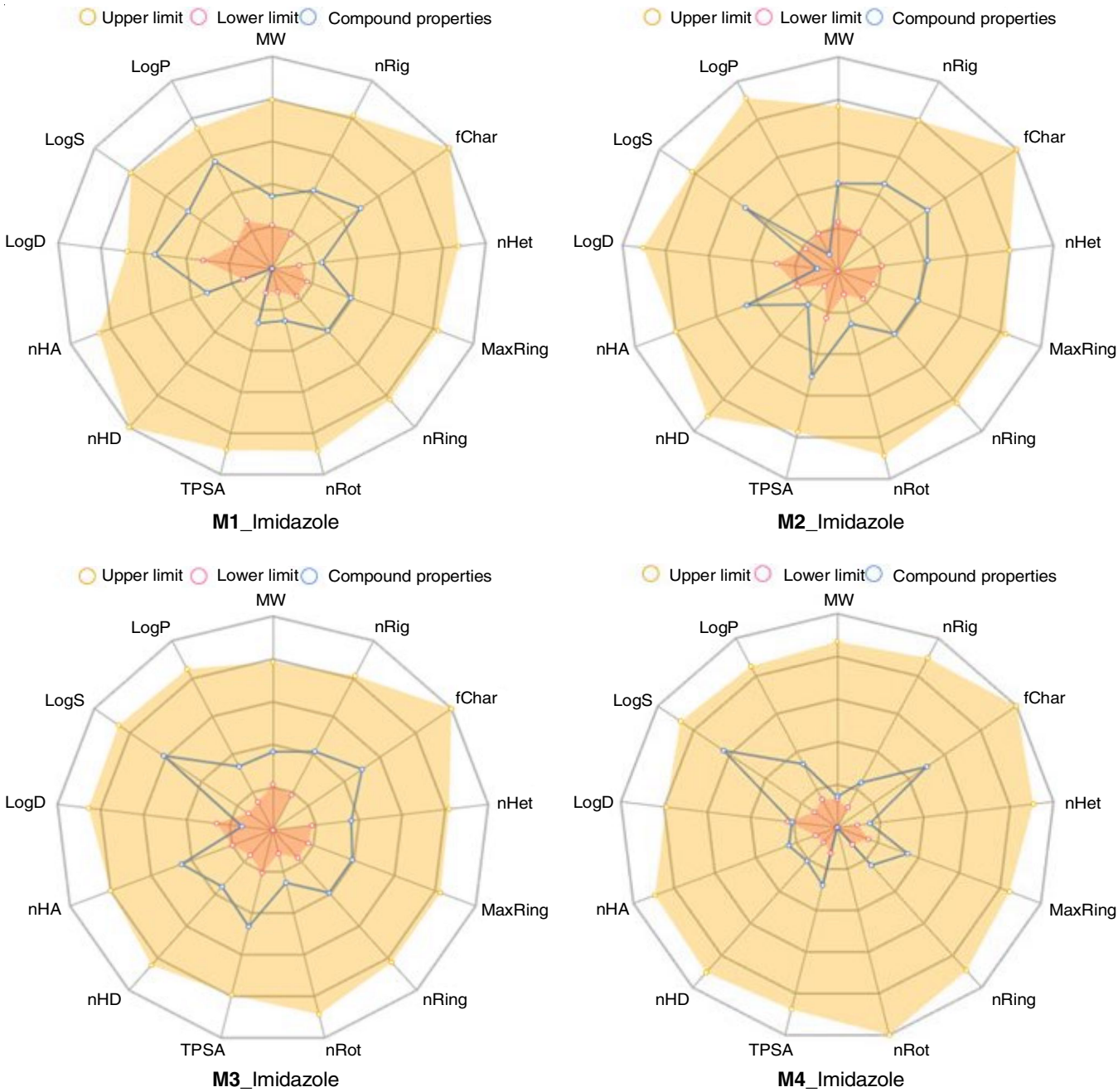

Fig. 8. Bioavailability radars showing the predicted range of physico-chemical parameters of the methyl-imidazole derivatives (**M1-M4**)

TABLE-4
LIPINSKI'S RULE PARAMETERS OF METHYL-IMIDAZOLE DERIVATIVES (**M1-M4**)

Compounds	M.W.	LogP	nHA	nHD	TPSA	nRT
M1	216.130	1.927	3	0	27.050	2
M2	266.070	-0.459	5	1	72.190	2
M3	233.120	0.799	5	2	61.520	2
M4	110.080	0.793	2	1	28.680	0

Table-6 presents a comprehensive overview of the pertinent established ADMET parameters including human cytochromes (CYP), clearance (CL), half-life ($T_{1/2}$), AMES toxicity, carcinogenicity (Carc), eye toxicity, Madin-Darby canine kidney cells (MDCK) permeability, plasma glycoprotein (Pgp) inhibitor, plasma glycoprotein (Pgp) substrate, plasma protein binding (PPB), volume distribution (VD), blood-brain barrier (BBB) penetration and human intestinal absorption (HIA). These parameters play a crucial role in assessing the pharmacokinetic and toxicological profiles of the compounds under investigation. Furthermore, significant observations were made regarding the methyl-imidazole derivatives (**M1**-**M4**), specifically their optimal

TABLE-5
THE METHYL-IMIDAZOLE DERIVATIVES (**M1-M4**) QUANTITATIVE DRUG-LIKENESS (QED), SYNTHETIC ACCESSIBILITY (SA) AND OTHER DRUG-LIKENESS RULES ARE ALSO ASSESSED. COMPARES COMPOUNDS' DRUG-LIKENESS BASED ON THEIR Ghose, Veber, Egan, Muegge, QED AND SA VALUES

Compounds	QED	SA	Ghose	Veber	Egan	Muegge
M1	0.771	1.911	Yes	Yes	Yes	Yes
M2	0.844	2.183	Yes	Yes	Yes	Yes
M3	0.782	2.687	Yes	Yes	Yes	Yes
M4	0.536	2.611	Yes	Yes	Yes	Yes

TABLE-6
ADMET PROPERTIES DATASET OF METHYL-IMIDAZOLE DERIVATIVES (**M1-M4**)

Category	Properties	Prediction probability values (Symbols)			
		M1	**M2**	**M3**	**M4**
Absorption	Human intestinal absorption (HIA)	0.007	0.053	0.038	0.023
	MDCK permeability	2.66e-05	1.42e-05	9.26e-06	1.38e-05
	Caco-2 permeability	-4.695	-4.942	-4.551	-4.721
	Pgp-inhibitor	0.001	0	0	0
	Pgp-substrate	0.009 (-)	0.044 (-)	0.955 (+)	0.014 (-)
	Plasma protein binding (PPB)	64.41%	45.68%	14.60%	55.30%
Distribution	The volume of distribution (VD)	1.06	0.401	0.468	1.26
	Blood brain barrier (BBB)	0.981 (+)	0.976 (+)	0.548 (+)	0.965 (+)
	CYP1A2 inhibitor	0.354 (-)	0.019 (- - -)	0.175 (- -)	0.321 (-)
	CYP1A2 substrate	0.938 (+++)	0.55 (+)	0.302(-)	0.949 (+++)
	CYP2C19 inhibitor	0.224 (- -)	0.043 (- - -)	0.053 (- - -)	0.038 (- - -)
	CYP2C19 substrate	0.922 (+++)	0.694 (+)	0.062 (- - -)	0.087 (- - -)
Metabolism	CYP2C9 inhibitor	0.013 (- - -)	0.002 (- - -)	0.004 (- - -)	0.007 (- - -)
	CYP2C9 substrate	0.559 (+)	0.337 (-)	0.704 (+)	0.07 (- - -)
	CYP2D6 inhibitor	0.058 (- - -)	0.006 (- - -)	0.001 (- - -)	0.206 (- -)
	CYP2D6 substrate	0.849 (++)	0.355 (-)	0.184 (- -)	0.316 (-)
	CYP3A4 inhibitor	0.119 (- - -)	0.009 (- - -)	0.009 (- - -)	0.014 (- - -)
	CYP3A4 substrate	0.911 (++)	0.494 (-)	0.085 (- - -)	0.565 (+)
Excretion	CL	7.943	2.872	9.561	6.849
	$T_{1/2}$	0.49	0.272	0.272	0.653
	AMES toxicity	0.5559 (+)	0.018 (- - -)	0.961 (+++)	0.018 (- - -)
Toxicity	Carcinogenicity	0.959 (+++)	0.959 (+++)	0.929 (+++)	0.952 (+++)
	Eye irritation	0.628 (+)	0.432 (-)	0.278 (- -)	0.982 (+)
	Respiratory toxicity	0.147 (- -)	0.929 (+ ++)	0.161 (- -)	0.936 (+++)

Key: The six symbols representing the prediction probability values are 0-0.1 (-), 0.1-0.3 (-), 0.3-0.5 (-), 0.5-0.7 (+), 0.7-0.9 (++) and 0.9-1.0 (+++). Typically, "+++" or "++" denotes a molecule that is more likely to be poisonous or flawed, while '-" or "- -" denotes a molecule that is appropriate or harmless.

Caco-2 permeability ranging from -4.551 to -4.942. The Caco-2 permeability, which is linked to enhance human intestinal absorption, demonstrated favourable values for these derivatives. A high Caco-2+ value indicates a higher rate of intestinal absorption for a medication. Remarkably, all the evaluated modeled compounds exhibited a promising likelihood of being absorbed through the intestinal membrane, as indicated by the calculated human intestinal absorption (HIA) values, which were consistently favourable.

Additionally, it was observed that the methyl-imidazole derivatives (**M1**-**M4**) possessed higher-than-average calculated values for blood-brain barrier (BBB) penetration. A favourable lipophilicity profile enables easy absorption from plasma membranes and contributes to a substance's ability to traverse the blood-brain barrier. All the methyl-imidazole derivatives (**M1**-**M4**) exhibited calculated BBB values denoted as BBB++, highlighting their favourable lipophilicity profile.

Plasma protein binding (PPB) is a crucial criterion in determining a drug's safety because medications with high PPB values (> 90%) have limited therapeutic indices, whilst those with low PPB values are significantly safer. Low PPB values indicate that certain drugs have a wide therapeutic index. Methyl-imidazole derivatives (**M1-M4**) were found to be carcinogenic in terms of their ability to cause cancer. The AMES toxicity profile showed that certain substances had a likelihood of being harmful. All compounds have positive values for the synthetic accessibility score (SA score), which is used to gauge how simple it is to synthesize molecules that are similar to those found in drugs. Overall, the ADMET profiles of all drugs improved. Moreover, the drug-likeness and ADMET predictions showed that they had good pharmacokinetic profiles and did not violate Lipinski's rule. The results of this theoretical investigation indicated potential lead compounds for subsequent *in silico* research of enhanced anticancer drugs [63].

Conclusion

In order to gain a deeper understanding of the inter- and intra-atomic interactions, stability and reactivity of a studied

compound with respect to its biological applications, the optimized ground state molecular structure was achieved through various theoretical methods. The DFT/B3LYP, B3PW91, M06-2X, PBE0 and ωB967X-D functional, along with the 6-311++g (d,p) basis set, were utilized to investigate geometry parameters, including bond length and bond angle, of the four studied compounds (**M1**-**M4**). The theoretical investigation revealed that the various substituent attachments gradually changed the bond length and bond angle of methyl-imidazole derivatives (**M1**-**M4**). This analysis can be utilized to predict the behaviour of molecules and provide information about their reactivity and characteristics. The HOMO-LUMO energy gap was also analyzed to observe the reactivity and stability of the studied compounds using different theoretical methods. For **M1**, the most stable method of theory was found to be ωB9X-D, with an energy gap value of 6.6573 eV. The HOMO was found to be highly concentrated on the imidazole ring in **M1**, while the LUMO was delocalized on the substituted benzene ring. Similar observations were made for compounds **M2**, **M4**, while for **M3**, the LUMO was delocalized at the benzene ring but the HOMO was concentrated on the attached substituent. The HYDE energy parameter was calculated using molecular docking and the biological activity values of methyl-imidazole derivatives (**M1**-**M4**) were compared. It was found that **M4** had the highest biological activity among them, while **M3** had the lowest. The increased biological activity of a compound is largely due to its larger surface area of contact with cancer proteins. The interaction between molecules and proteins is enhanced by increased molecule contact surface. The AMES toxicity profile showed that certain substances had a likelihood of being harmful, while the ADMET profiles of all drugs improved. The theoretical investigation indicated potential compounds for subsequent *in silico* research of enhanced anticancer drugs. The use of various theoretical methods to analyse the inter- and intra-atomic interactions, stability and reactivity of the studied compounds has provided valuable insights into its biological applications and potential as an anticancer drug.

ACKNOWLEDGEMENTS

Two of the authors, S. Koudjina and J.A. Agwupuye, thank all the collaborators in University of Calabar in Nigeria and UNSTIM of Abomey in Benin for a fruitful discussion and a good sense of work well done, *via* the intensive computing equipment available to us.

CONFLICT OF INTEREST

The authors declare that there is no conflict of interests regarding the publication of this article.

REFERENCES

1. Y. Yuan, S. Majumder, M. Yang and S.R. Guo, *Tetrahedron Lett.*, **61**, 151506 (2020); https://doi.org/10.1016/j.tetlet.2019.151506
2. I. Ali, M.N. Lone and H.Y. Aboul-Enein, *MedChemComm*, **8**, 1742 (2017); https://doi.org/10.1039/C7MD00067G
3. A. Rammohan, B.V. Bhaskar and G.V. Zyryanov, in eds.: P. Singh, Recent Developments in the Synthesis of Pyridine Analogues as a Potent Anti-Alzheimer's Therapeutic Leads, In: Recent Developments in the Synthesis and Applications of Pyridines, Elsevier, Chap. 13, pp. 411-444 (2023); https://doi.org/10.1016/B978-0-323-91221-1.00009-9
4. A.M. Abu-Dief, L.H. Abdel-Rahman, A.A. Abdelhamid, A.A. Marzouk, M.R. Shehata, M.A. Bakheet, O.A. Almaghrabi and A. Nafady, *Spectrochim. Acta A Mol. Biomol. Spectrosc.*, **228**, 117700 (2020); https://doi.org/10.1016/j.saa.2019.117700
5. N. Kumar and N. Goel, *Phys. Sci. Rev.*., **8**, 2903 (2021); https://doi.org/10.1515/psr-2021-0041
6. Y. Chen, K. Tao, W. Ji, V.B. Kumar, S. Rencus-Lazar and E. Gazit, *Mater. Today*, **60**, 106 (2022); https://doi.org/10.1016/j.mattod.2022.08.011
7. N. Behera and V. Manivannan, *ChemistrySelect*, **1**, 4016 (2016); https://doi.org/10.1002/slct.201600799
8. I. Tabushi and Y. Kuroda, *J. Am. Chem. Soc.*, **106**, 4580 (1984); https://doi.org/10.1021/ja00328a047
9. U. Eduok, O. Faye and J. Szpunar, *RSC Adv.*, **6**, 108777 (2016); https://doi.org/10.1039/C6RA23099G
10. P. Lienard, J. Gavartin, G. Boccardi and M. Meunier, *Pharm. Res.*, **32**, 300 (2015); https://doi.org/10.1007/s11095-014-1463-7
11. N.J. Britto, M. Jaccob, P. Comba, K. Anandababu and R. Mayilmurugan, *J. Inorg. Biochem.*, **238**, 112066 (2023); https://doi.org/10.1016/j.jinorgbio.2022.112066
12. V.M. Rayón, H. Valdés, N. Díaz and D. Suárez, *J. Chem. Theory Comput.*, **4**, 243 (2008); https://doi.org/10.1021/ct700229e
13. K. Boussouf, R. Boulmene, M. Prakash, N. Komiha, M. Taleb, M.M. Al-Mogren and M. Hochlaf, *Phys. Chem. Chem. Phys.*, **17**, 14417 (2015); https://doi.org/10.1039/C4CP06108J
14. O.M.H. Salo-Ahen, I. Alanko, R. Bhadane, A.M.J.J. Bonvin, R.V. Honorato, S. Hossain, A.H. Juffer, A. Kabedev, M. Lahtela-Kakkonen, A.S. Larsen, E. Lescrinier, P. Marimuthu, M.U. Mirza, G. Mustafa, A. Nunes-Alves, T. Pantsar, A. Saadabadi, K. Singaravelu and M. Vanmeert, *Processes*, **9**, 71 (2020); https://doi.org/10.3390/pr9010071
15. A.R. Leach, Molecular Modelling: Principles and Applications. Pearson Education Limited. Edinburgh Gate, Harlow, Essex CM20 2JE (2001).
16. W.F. Van Gunsteren and H.J. Berendsen, *Angew. Chem. Int. Ed. Engl.*, **29**, 992 (1990); https://doi.org/10.1002/anie.199009921
17. M.A. Saller, A. Kelly and E. Geva, *J. Phys. Chem. Lett.*, **12**, 3163 (2021); https://doi.org/10.1021/acs.jpclett.1c00158
18. E. Bremond, I. Ciofini, J.C. Sancho-García and C. Adamo, *Acc. Chem. Res.*, **49**, 1503 (2016); https://doi.org/10.1021/acs.accounts.6b00232
19. E. Torres and G.A. DiLabio, *J. Phys. Chem. Lett.*, **3**, 1738 (2012); https://doi.org/10.1021/jz300554y
20. M. Blaško, L.F. Pašteka and M. Urban, *J. Phys. Chem. A*, **125**, 7382 (2021); https://doi.org/10.1021/acs.jpca.1c04793
21. E.A. Eno, H. Louis, P. Ekoja, I. Benjamin, S.A. Adalikwu, M.M. Orosun, T.O. Unimuke, F.C. Asogwa and E.C. Agwamba, *J. Indian Chem. Soc.*, **99**, 100532 (2022); https://doi.org/10.1016/j.jics.2022.100532
22. R. Peverati and D.G. Truhlar, *J. Chem. Theory Comput.*, **8**, 2310 (2012); https://doi.org/10.1021/ct3002656
23. M.J. Frisch, G.W. Trucks, H.B. Schlegel, G.E. Scuseria, M.A. Robb, J.R. Cheeseman, G. Scalmani, V. Barone, G.A. Petersson, H. Nakatsuji, X. Li, M. Caricato, A.V. Marenich, J. Bloino, B.G. Janesko, R. Gomperts, B. Mennucci, H.P. Hratchian, J.V. Ortiz, A.F. Izmaylov, J.L. Sonnenberg, D. Williams Young, F. Ding, F. Lipparini, F. Egidi, J. Goings, B. Peng, A. Petrone, T. Henderson, D. Ranasinghe, V.G. Zakrzewski, J. Gao, N. Rega, G. Zheng, W. Liang, M. Hada, M. Ehara, K. Toyota, R. Fukuda, J. Hasegawa, M. Ishida, T. Nakajima, Y. Honda, O. Kitao, H. Nakai, T. Vreven, K. Throssell and J.A. Montgomery Jr, J.E. Peralta, F. Ogliaro, M.J. Bearpark, J.J. Heyd, E.N. Brothers, K.N. Kudin, V.N. Staroverov, T.A. Keith, R. Kobayashi, J. Normand, A.P.

Rendell, K. Raghavachari, J.C. Burant, S.S. Iyengar, J. Tomasi, M. Cossi, J.M. Millam, M. Klene, C. Adamo, R. Cammi, J.W. Ochterski, R.L. Martin, K. Morokuma, O. Farkas, J.B. Foresman and D.J. Fox, Gaussian 16, Revision B.01, Gaussian, Inc., Wallingford CT (2016).
24. R. Dennington, T.A. Keith and J.M. Millam, GaussView 6.0. 16. Semichem Inc.: Shawnee Mission, KS, USA (2016).
25. T. Tsuneda, J.-W. Song, S. Suzuki and K. Hirao, *J. Chem. Phys.*, **133**, 174101 (2010); https://doi.org/10.1063/1.3491272
26. S. Grimme, S. Ehrlich and L. Goerigk, *J. Comput. Chem.*, **32**, 1456 (2011); https://doi.org/10.1002/jcc.21759
27. S. Grimme, J. Antony, S. Ehrlich and H. Krieg, *J. Chem. Phys.*, **132**, 154104 (2010); https://doi.org/10.1063/1.3382344
28. S. Grimme, *J. Comput. Chem.*, **27**, 1787 (2006); https://doi.org/10.1002/jcc.20495
29. J.P. Perdew, M. Ernzerhof and K. Burke, *J. Chem. Phys.*, **105**, 9982 (1996); https://doi.org/10.1063/1.472933
30. X.H. Li, Z.X. Tang and X.Z. Zhang, *Int. J. Quantum Chem.*, **110**, 1565 (2010); https://doi.org/10.1002/qua.22295
31. F. Weinhold, *J. Comput. Chem.*, **33**, 2363 (2012); https://doi.org/10.1002/jcc.23060
32. LeadIT version 12.1.0; BioSolveIT GmbH, Sankt Augustin, Germany, (2023).
33. I. Akinwumi, A. Faleti, A. Owojuyigbe, F. Raji and M. Alaka, *J. Adv. Pharm. Res.*, **6**, 107 (2022); https://doi.org/10.21608/aprh.2022.139794.1175
34. Z. Nawaz, N. Riaz, M. Saleem, A. Iqbal, S.A. Ejaz, S. Muzaffar, B. Bashir, M. Ashraf, A. Rehman, M.S. Bilal, B.K. Prabhala and S. Sajid, *Heliyon*, **10**, e35278 (2024); https://doi.org/10.1016/j.heliyon.2024.e35278
35. V. Gapsys, A. Yildirim, M. Aldeghi, Y. Khalak, D. van der Spoel and B.L. de Groot, *Commun. Chem.*, **4**, 61 (2021); https://doi.org/10.1038/s42004-021-00498-y
36. L. Côrte-Real, V. Pósa, M. Martins, R. Colucas, N.V. May, X. Fontrodona, I. Romero, F. Mendes, C. Pinto Reis, M.M. Gaspar, J.C. Pessoa, É.A. Enyedy and I. Correia, *Inorg. Chem.*, **62**, 11466 (2023); https://doi.org/10.1021/acs.inorgchem.3c01066
37. P.A. Nikitina and V.P. Perevalov, *Chem. Heterocycl. Comp.*, **53**, 123 (2017); https://doi.org/10.1007/s10593-017-2030-z
38. A. Sharma, V. Kumar, R. Kharb, S. Kumar, P.C. Sharma and D.P. Pathak, *Curr. Pharm. Design*, **22**, 3265 (2016); https://doi.org/10.2174/1381612822666160226144333
39. P.R. Varadwaj, A. Varadwaj, H.M. Marques and K. Yamashita, *Int. J. Mol. Sci.*, **23**, 1263 (2022); https://doi.org/10.3390/ijms23031263
40. G.V. Gibbs, F.C. Hawthorne and G.E. Brown Jr., *Am. Mineral.*, **107**, 1219 (2022); https://doi.org/10.2138/am-2021-7938
41. X. Fang, L. Liu, J. Lei, D. He, S. Zhang, J. Zhou, F. Wang, H. Wu and H. Wang, *Nat. Mach. Intell.*, **4**, 127 (2022); https://doi.org/10.1038/s42256-021-00438-4
42. J.A. Agwupuye, H. Louis, T.E. Gber, I. Ahmad, E.C. Agwamba, A.B. Samuel, E.J. Ejiako, H. Patel, I.T. Ita and V.M. Bassey, *Chem. Phys. Impact*, **5**, 100122 (2022); https://doi.org/10.1016/j.chphi.2022.100122
43. J.A. Agwupuye, T.E. Gber, H.O. Edet, M. Zeeshan, S. Batool, O.E.E. Duke, P.O. Adah, J.O. Odey and G.E. Egbung, *Chem. Phys. Impact*, **6**, 100146 (2023); https://doi.org/10.1016/j.chphi.2022.100146
44. A. Zochedh, M. Priya, A. Shunmuganarayanan, K. Thandavarayan and A.B. Sultan, *J. Mol. Struct.*, **1268**, 133651 (2022); https://doi.org/10.1016/j.molstruc.2022.133651
45. J.A. Agwupuye, H. Louis, T.O. Unimuke, P. David, E.I. Ubana and Y.L. Moshood, *J. Mol. Liq.*, **337**, 116458 (2021); https://doi.org/10.1016/j.molliq.2021.116458
46. M.I. Ofem, H. Louis, J.A. Agwupuye, U.S. Ameuru, G.C. Apebende, T.E. Gber, J.O. Odey, N. Musa and A. Ayi, *BMC Chem.*, **16**, 109 (2022); https://doi.org/10.1186/s13065-022-00896-w
47. M.D. Mohammadi, F. Abbas, H. Louis, L.E. Afahanam and T.E. Gber, *ChemistrySelect*, **7**, e202202535 (2022); https://doi.org/10.1002/slct.202202535
48. T.E. Gber, H. Louis, A.E. Owen, B.E. Etinwa, I. Benjamin, F.C. Asogwa, M.M. Orosun and E.A. Eno, *RSC Adv.*, **12**, 25992 (2022); https://doi.org/10.1039/D2RA04028J
49. J.A. Agwupuye, H. Louis, O.C. Enudi, T.O. Unimuke and M.M. Edim, *Mater. Chem. Phys.*, **275**, 125239 (2022); https://doi.org/10.1016/j.matchemphys.2021.125239
50. A. El-Rayyes, R. T. Mogharbel, M. H. Abdel-Rhman, M. A. Ismail and E. Abdel-Latif, *Bull. Chem. Soc. Ethiop.*, **37**, 1275 (2023); https://doi.org/10.4314/bcse.v37i5.18
51. J.P. Wagner and P.R. Schreiner, *Angew. Chem. Int. Ed.*, **54**, 12274 (2015); https://doi.org/10.1002/anie.201503476
52. P. Csermely, T. Korcsmáros, H.J. Kiss, G. London and R. Nussinov, *Pharmacol. Ther.*, **138**, 333 (2013); https://doi.org/10.1016/j.pharmthera.2013.01.016
53. N.A. Dashatan, M.R. Tavirani, H. Zali, M. Koushki and N. Ahmadi, *Galen Med. J.*, **7**, e1129 (2018); https://doi.org/10.31661/gmj.v7i0.1129
54. Y. Riadi, M.H. Geesi, S.A. Ejaz, O. Afzal and A. Oubella, *J. Mol. Struct.*, **1322**, 140420 (2025); https://doi.org/10.1016/j.molstruc.2024.140420
55. M. Aziz, S.A. Ejaz, N. Tamam, F. Siddique, N. Riaz, F.A. Qais, S. Chtita and J. Iqbal, *Sci. Rep.*, **12**, 6404 (2022); https://doi.org/10.1038/s41598-022-10253-5
56. J. Porter, S. Lumb, F. Lecomte, J. Reuberson, A. Foley, M. Calmiano, K. le Riche, H. Edwards, J. Delgado, R.J. Franklin, J.M. Gascon-Simorte, A. Maloney, C. Meier and M. Batchelor, *Bioorg. Med. Chem. Lett.*, **19**, 397 (2009); https://doi.org/10.1016/j.bmcl.2008.11.062
57. Y. Amano, T. Yamaguchi, T. Niimi and H. Sakashita, *Acta Crystallogr. D Biol. Crystallogr.*, **71**, 918 (2015); https://doi.org/10.1107/S1399004715002175
58. W. Qiu, M. Zhou, F. Labrie and S.X. Lin, *Mol. Endocrinol.*, **18**, 1798 (2004); https://doi.org/10.1210/me.2004-0032
59. M. Zhang, Y. Zhang, M. Song, X. Xue, J. Wang, C. Wang, C. Zhang, C. Li, Q. Xiang, L. Zou, X. Wu, C. Wu, B. Dong, W. Xue, Y. Zhou, H. Chen, D. Wu, K. Ding and Y. Xu, *J. Med. Chem.*, **61**, 3037 (2018); https://doi.org/10.1021/acs.jmedchem.8b00103
60. A. Kosiha, K.M. Lo, C. Parthiban and K.P. Elango, *Mater. Sci. Eng. C*, **94**, 778 (2019); https://doi.org/10.1016/j.msec.2018.10.021
61. L. Ozalp, S.S. Erdem, B. Yüce-Dursun, Ö. Mutlu and M. Özbil, *Comput. Biol. Chem.*, **77**, 87 (2018); https://doi.org/10.1016/j.compbiolchem.2018.09.009
62. S.H. Abdullahi, A. Uzairu, G.A. Shallangwa, S. Uba and A.B. Umar, *Chemistry Africa*, **6**, 1381 (2023); https://doi.org/10.1007/s42250-023-00592-9
63. A. Ahmed, A. Saeed, S.A. Ejaz, M. Aziz, M.Z. Hashmi, P.A. Channar, Q. Abbas, H. Raza, Z. Shafiq and H.R. El-Seedi, *RSC Advances*, **12**, 11974 (2022); https://doi.org/10.1039/D1RA09318E